SiGe/Si(001) Stranski-Krastanow islands by liquid-phase epitaxy: Diffuse x-ray scattering versus growth observations

M. Hanke, M. Schmidbauer, D. Grigoriev, H. Raidt, P. Schäfer, and R. Köhler

Institut für Physik, Humboldt-Universität zu Berlin, Newtonstrasse 15, D-12489 Berlin

A.-K. Gerlitzke and H. Wawra

Institut für Kristallzüchtung, Max-Born-Strasse 2, D-12489 Berlin, Germany

Ex situ observed growth stages of LPE-SiGe/Si(001) Stranski-Krastanow islands with a germanium content of 10% give clear evidence of a rapid shape transition at one third of the final island height. The island shape changes from a lenslike type without a top facet to truncated pyramids with {111} side facets and an (001) top facet. High-resolution x-ray diffraction has been applied to islands with higher germanium content of about 30%. Experimental results are compared with respective kinematical scattering simulations based on finite element calculations for the strain field. From these simulations the three-dimensional germanium composition profile inside the islands can be extracted and it substantiates a similar growth scenario with a distinct shape transition at one third of the final island height also for this germanium concentration range. We attribute the observed finite island size to a distinct nucleation problem at the island bottom caused by exceptional high strain energy around the island corners in combination with a strain driven wetting layer depression.

I. INTRODUCTION

In the past decade ambitious efforts have been undertaken for the fabrication and investigation of low-dimensional semiconductor structures. As soon as a charge carrier is spatially confined to lateral dimensions smaller than the DeBroglie wavelength the according density of states will drastically change with respect to bulk material, which promises new fascinating electronical and optical properties. In principle, the confinement can be obtained in one, two, or even three dimensions. Quantum dots (QD) with zero-dimensional properties represent the outmost degree of confinement predestinating them for exceptional optoelectronical devices as quantum dot lasers,[1] single electron transistors,[2] or single electron memory devices.[3]

For the fabrication of zero-dimensional structures of high density along with outstanding degree of uniformity the Stranki-Krastanow (SK) growth mode[4] has been widely used for different material combinations. The accumulated deformation energy during heteroepitaxial growth can be partially relieved by forming three-dimensional dislocation-free islands on top of a wetting layer because the energy reduction associated with elastic relaxation exceeds the increase in surface energy.

A purposeful fabrication and application requires a detailed understanding of the growth process. Therefore there is a practical need for precise characterization of morphological properties as shape, size, chemical composition, and strain profile. A large variety of direct and indirect methods have been applied, among them scanning probe techniques as atomic force microscopy (AFM) (Refs. 5 and 6) and scanning tunneling microscopy. Furthermore scanning electron microscopy (SEM) as well as transmission electron microscopy (Ref. 7) can reveal reliable structural properties. Further on Raman scattering can provide information concerning composition and strain in free standing and capped islands.[8]

However, all the direct methods can provide structural information only for a comparatively limited number of objects. Indirect methods are able to compensate this lack in a complementary way, although reliable information regarding a particular individual type will be available only in case of a monodisperse distribution.

High-resolution x-ray diffraction (HRXRD) has been widely used for strain analysis in QD's, e.g.,[9–16] which confirms the important role of interdiffusion as an effective way of elastic relaxation during growth. Previously, different germanium profiles within free standing SiGe SK islands have been proposed: a linear increase of germanium for islands on a Si(111) substrate,[14] a quadratic increase in case of SiGe/Si(001) islands[17] and a stepped germanium profile.[10,18] Recently, Denker *et al.*[19] have reported on a lateral composition profile inside self-assembled SiGe dots on Si(001). By selective etching technique the authors observed a strong silicon intermixing in the island corners, whereas the edges, the island top and the inner part of the island remain germanium rich. Lateral transport governed by three-dimensional strain distribution and local incorporation probabilities have been discussed in addition as further key parameters for the final concentration profile within SK islands.[20]

In the present paper we will reconstruct how island evolution in the system SiGe/Si(001) takes place in detail. We got evidence for a characteristic growth transition at $h/3$, which can be directly interconnected to a certain germanium profile depending on the particular growth mode. We could trace the island evolution by different growth stages only in case of comparatively low germanium contents. Since islands with a higher lattice mismatch with respect to the substrate material grow increasingly faster, there is no direct access to different stages of growth. From HRXRD experiments along with various kinematical scattering simulations, which reveal a certain germanium profile we argue that even in that case the proposed growth scenario remains the same.

Furthermore we will focus on the rather frequently discussed question why the observed only misfit dependent final island size[21] keeps finite. We will explain this in terms of a sustainable nucleation problem at the island bottom along with a wetting layer depression.

The present paper is organized as follows. An introduction to the simulation procedure will be given in the following section. Section III briefly describes sample preparation. Section IV refers to the experimental setup and the applied scattering techniques, whereas in Sec. V concentration profiles revealed by respective simulations will be discussed versus direct growth observations. Finally, in Sec. VI we will present our conclusions.

II. THEORY

Kinematical scattering simulations have been performed in order to evaluate the diffusely scattered intensity patterns. Although different groups pursue analytical methods to calculate the strain field, e.g., within buried[22] and freestanding quantum wires,[23] hut clusters,[17] QD's with rotational symmetry,[24] and buried SiGe/Si QD's neglecting the elastic anisotropy[25] there is still a lack of analytical solutions for the strain field within mesoscopic structures taking into account the elastic properties. Alternatively, numerical finite element method (FEM) is as a very powerful tool for strain analysis. It has been widely used for mesoscopic structures.[7,18,26,27]

Island shape and size serve as input parameters for FEM calculation[28] as well as composition profile, corresponding lattice parameters and the elastic constants c_{ijkl} for $Si_{1-x}Ge_x$ assuming Vegard's law.[29] Shape and size have been previously determined by direct methods. A wetting layer of constant 2 nm thickness has been considered within the FEM model. Previous investigations confirm a strong elastic interaction between substrate and island. It has been shown that there is a remarkable influence to the strain profile into the substrate at least down to a depth equivalent to the island height.[30] Thus, according to the concrete geometry of the investigated islands lateral and vertical dimensions of the entire model are 260 nm and 100 nm, respectively, which ensure a realistic elastic behavior. To establish quasiperiodic boundary conditions the FEM nodes within the outermost planes of the substrate have the freedom to exclusively relax within those planes.

Since finite element method is a continuum theory it remains still impossible to take an atomistic structure of mesoscopic objects correctly into account. Consequently, we have to simplify the model defining FEM cells with typical dimensions between 5 Å and 50 Å. Usually the grid has to be arranged more dense in areas with high strain energy, e.g., at the interface island/wetting layer and near the edges. In an intermediate step the deformation field has to be interpolated onto a regular grid of a mesh size d which is usually still larger than an interatomic distance corresponding to supercells. However, this treatment is only valid under the assumption that the local displacement $\vec{u}$ within a supercell is negligible with respect to the displacement of the supercell itself, thus

$$\vec{u}(\vec{R}_i + \vec{r}_k) \approx \vec{u}(\vec{R}_i), \qquad (1)$$

where $\vec{R}_i$ is the position of the ith supercell. $\vec{r}_k$ denotes the position of the kth atom in the supercell. In general the diffusely scattered amplitude $A_{diffuse}$ can be calculated as a coherent sum over all illuminated scatterers,

$$A_{diffus}(\vec{q}) \propto \sum_i \sum_k \{\varrho^{ideal}(\vec{R}_i + \vec{r}_k)\exp[i\vec{q}[(\vec{R}_i + \vec{r}_k)$$
$$+ \vec{u}(\vec{R}_i + \vec{r}_k)]] - \varrho^{ref}(\vec{R}_i + \vec{r}_k)\exp[i\vec{q}(\vec{R}_i + \vec{r}_k)]\}, \qquad (2)$$

where ϱ^{ref} and ϱ^{ideal} are electron densities of an *ideal* and a *reference* lattice, respectively. It has to be noted that most of the intensity has to be treated dynamically. Whereas only a small fraction—the scattering by highly distorted parts of the crystal—can be calculated kinematically. It was shown[31] that in our case the chemical composition within an island de facto exclusively enters the diffuse scattering via a certain strain profile $\vec{u}(\vec{R})$ and not directly by the atomic form amplitudes. A detailed discussion of this treatment has been published elsewhere.[18]

III. SAMPLE PREPARATION

The samples were grown with liquid phase epitaxy (LPE) using a slide-boat reactor. In contrast to other growth techniques as molecular beam epitaxy (MBE) or metal organic chemical vapor deposition LPE operates comparatively closer to thermodynamical equilibrium. Consequently, LPE-grown islands exhibit a similar shape for an extended concentration range which consists of truncated pyramids with {111} side facets and an (001) top facet with a nearly constant aspect ratio of island base along [110] to island height of two.

To ensure a high purity of the epitaxial layers the entire growth process has to be performed under a pure hydrogen atmosphere. In a first step the components Si and Ge are solved in a Bi-solution which will be homogenized for several hours at growth temperature of 973 K to equilibrate the system thermodynamically. Averaged germanium contents of 9% (sample shown in Fig. 4) and 30% [for diffuse scattering see Fig. 5(b)] in the solid phase correspond to germanium mol fractions of 0.0046 and 0.0103 in the liquid phase, respectively. After *in situ* desorption of the natural oxid layer at 930 °C the Si-Ge-Bi solution is brought into contact with the substrate material. To initialize the growth an oversaturation was established by choosing a growth temperature up to 2 K below saturation temperature.

IV. EXPERIMENT

Direct imaging techniques as AFM and SEM have been applied to characterize morphological properties like island size and shape. HRXRD and grazing incidence small angle x-ray scattering have been used to get access to inherent properties as concentration and strain profiles. X-ray scattering experiments were performed by using synchrotron radia-

tion as provided by BW2 station at Hasylab (DESY) using a monochromatized well collimated beam with an x-ray energy of 8 keV and a typical energy band width of $\Delta\lambda/\lambda = 10^{-4}$. Typical beam spots are 0.5 mm by 2 mm with respective beam divergences within and perpendicular the scattering plane of 50 μrad and 200 μrad. A linear position sensitive detector with a spatial resolution of 80 μm was placed 750 mm behind the sample, whereas the resolution perpendicular to the scattering plane amounts to 4×10^{-3} Å^{-1}.

V. RESULTS AND DISCUSSION

A. Island evolution

Elastic lattice relaxation during heteroepitaxial growth may occur through the transition from a flat surface to an undulated surface. In case of $Si_{1-x}Ge_x/Si(001)$ the originating pattern exhibits preferential directions along the elastically soft $\langle 100 \rangle$ directions of the cubic diamond lattice. It has been shown that during later growth stages separated islands appear exactly at the crest of the ripple pattern. Thus, the final island positions have been discussed in terms of a ripple pattern.[32] However, positional correlation could also be found in case of high Ge content ($x > 0.15$)—within a concentration window without a proof of a ripple pattern.

Since at lower Ge contents a variety of different island stages remain at the surface a *postgrowth* analysis opens a detailed morphological view to the island evolution. The reconstructed sequence can be subdivided into three main stages, Fig. 1. At the very beginning initial island stages (a) arise from a tiny surface undulation by increasingly steeper boundary planes up to an inclination angle of $\approx 16.9°$, which nearly corresponds to {115}-type facets (15.8°). During this first step no top facets are present and the islands exhibit a lenslike shape. Once {115} facets are present the island shape undergoes a rapid change by forming truncated pyramids with an (001) top facet, {111} side facets, and a quadratic base. With respect to the final island height h the growth mode alters exactly at $h/3$. However, this transition happens as fast as nonintermediate stage could be observed. There are two conceivable scenarios: (i) either the growth performs by different side facets down to {111} or (ii) there is vertical growth along (001) filling up the volume between previous {115} and final {111}. In the following section we will present results clearly indicating path (ii). At the end of transition ($a \Rightarrow b$) truncated pyramids with {111} side facets and an (001) top facet have evolved. It should be mentioned that the island base width slightly decreases during this step. Finally—after an (001) facet is present—the growth almost exclusively takes place vertically. However, there is also a lateral island broadening, whose microscopic nature throw light to the phenomenon of a finite island size.

The characteristic scaling law[21] for the final island size $w \propto x^{-2.03}$ is frequently discussed in terms of an inverse quadratic strain dependence. Regions of comparatively high strain energy tend to be resolved during subsequent growth and can serve as a monitor of strain distribution. Figure 2 shows a typical cloverleaflike wetting layer depression in the vicinity of a $Si_{0.9}Ge_{0.1}$ island, whose particular shape reflects the fourfold symmetry of the strain energy distribution, see
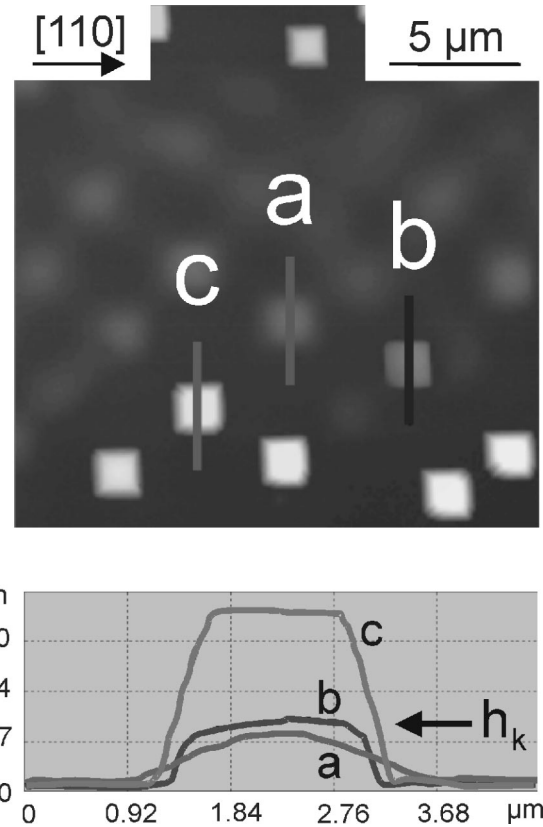

FIG. 1. Atomic force micrograph (top) and corresponding height profiles (bottom) taken on a sample with a comparatively low germanium content of 10%. A large variety of different island shapes and sizes has been recognized at special growth conditions. At a critical height the shape changes rapidly from a flat lens type (a) to truncated pyramids (b). Afterwards the growth happens along (001) (c).

Fig. 3(b). Strain induced wetting layer depression has also been observed for MBE and other material systems.[5,33–36] Figure 4 depicts a fully developed $Si_{0.91}Ge_{0.09}$ island with a final aspect ratio island base/height of nearly two. The image clearly reveals the microstructure of the $\langle 101 \rangle$ edges, which are made of small {111}-type facets.

Thus, the lateral island dimension still increases after formation of a truncated pyramid due to additional {111} slabs. Because there is no two-dimensional nucleation at {111} subsequent slabs exclusively nucleate at the island bottom. However, they do not grow into spatially complete facets since they stop in the island's corners at the bottom. FEM calculations predict a strongly enhanced strain energy nearby these corners, see Fig. 3(a), indicating a reason that the growth process initially suspends around these points. Later on nucleation will be completely suppressed after a strain induced wetting layer depression. For MBE grown islands it has been shown[5] that the depth of a wetting layer depression linearly scales with island diameter and self-limits after a certain island size is achieved. Taking both, the observed wetting layer depression and the calculated enhanced strain energy around the island corners, into account the final island size can be explained rather in terms of a kinetically caused nucleation problem than a transport phenomenon. We pre-
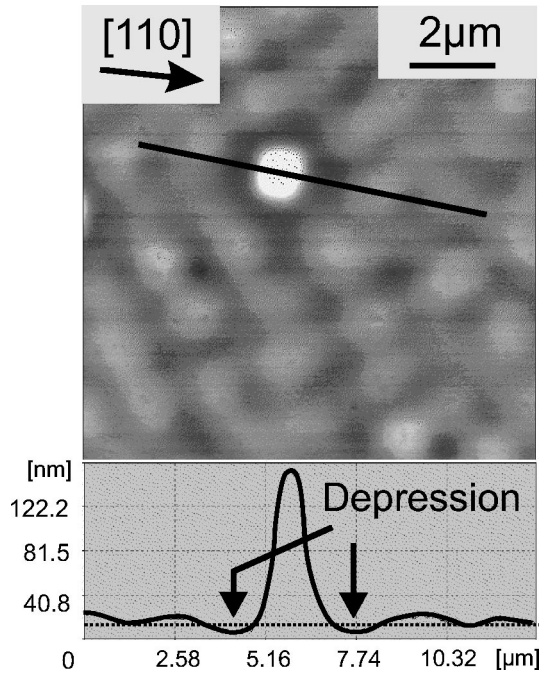
FIG. 2. Atomic force micrograph of a sample containing 10% germanium. Due to high strain energy in the vicinity of an island the wetting layer was depressed. Lateral dimension of this depression is in the order of the island size itself.

sume that the absence of further nucleation even holds as a key argument to a finite SK-island size in case of other growth techniques.

B. High-resolution x-ray diffraction

In the preceding section we have proposed a three-step island nucleation process reconstructed from *direct* imaging. There is a strong indication that at $\approx h/3$ the growth mechanism distinctly changes from a rough growth mode (corresponding to lenslike island shapes) towards a faceted one (truncated pyramids). In case of $x > 0.15$ a direct view to temporary morphological stages gets impossible, because an individual island passes extremely fast through subsequent stages, inducing island ensembles of high monodispersity.
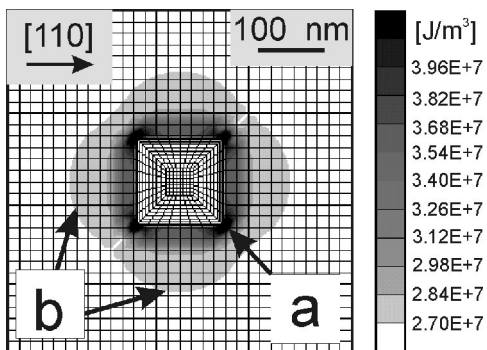

FIG. 3. Finite element calculation of the strain energy density in vicinity of a $Si_{0.7}Ge_{0.3}/Si(001)$ island, (a) denotes regions of an increased strain energy density and (b) the typical fourfold symmetry of the far field.
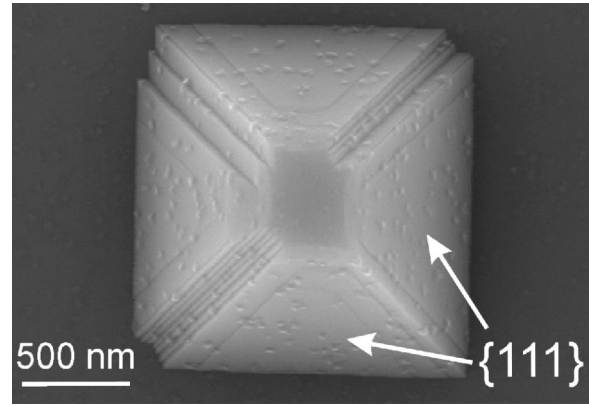

FIG. 4. Scanning electron micrograph of a $Si_{0.91}Ge_{0.09}/Si(001)$ island. The $\langle 101 \rangle$-edges show a pronounced dissection indicating to a suspended nucleation at the island bottom.

However, diffuse x-ray scattering can be applied as an excellent tool to reveal structural details of the island evolution. Since the actual growth mechanism significantly influences the amount of germanium incorporated a growth scenario could be deduced from a certain concentration profile. Further reasons for an inhomogeneous germanium profile could be an anisotropic incorporation probability, strain dependent lateral transport, and an impact of the actual moment of evolution, which directly refers to a time-dependent composition within the solution. Namely, the last point attracts particular interest since atomic force micrographs of a sample containing locally different island densities prove a sequential nucleation, where the islands appear one after another in chains along $\langle 100 \rangle$ directions at the end of an already existing formation.[37]

We investigated two-dimensional intensity distributions around symmetrical as well as asymmetrical reciprocal lattice points applying HRXRD. Figure 5(b) shows the measured intensity distribution around the Si(004) reciprocal lattice point, which will actually appear out of the measured area (at $q_{001} = 4.628$ Å^{-1}), whereas the cloud of diffuse intensity originates mainly from the scattering at coherently strained SiGe islands. It contains information regarding island size and shape as well as strain state, chemical composition, and positional correlation.

Lateral ordering satellites nearby the crystal truncation rod have been observed up to third order indicating a high degree of island correlation along the $\langle 100 \rangle$ direction. The averaged peak distance of $\Delta q = 0.0022$ Å^{-1} corresponds to $\Lambda = 285$ nm, which coincides with the island-island spacing within an island chain detected by AFM. The convolution theorem states that the diffusely scattered intensity by an ensemble of equivalent objects gets a simple product of diffuse scattering by a single individual times an interference function. Thus, regardless of correlation effects, scattering from an island ensemble can be treated exactly the same way as a single individual scattering process.

As a final outcome of an iterative evaluation process considering various island shapes and concentration profiles we will present two kinematical scattering simulations [Figs. 5(a) and 5(c)] which basically refer to exactly the same is-
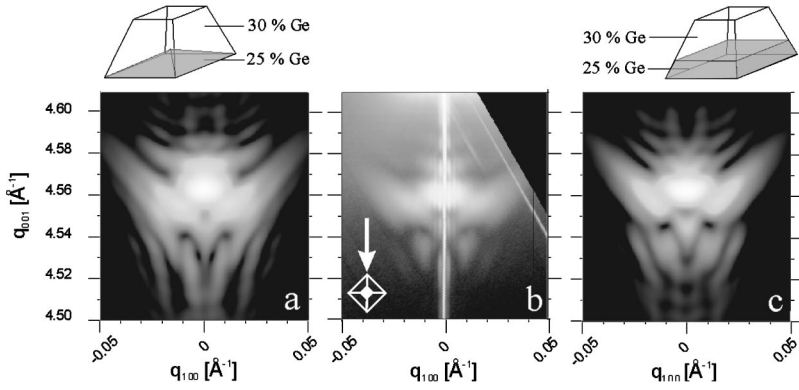
FIG. 5. Diffusely scattered intensity around 004 reflection (a) and (c) kinematical simulations for different models and (b) respective measurement. The strong feature on the right-hand side in (b) is caused by a detector artefact.

land shape revealed by AFM: a truncated pyramid with {111} side facets and an (001) top facet with a base width along [110] and height of 130 nm and 65 nm, respectively. However, the considered Ge distributions slightly differ regarding the two possible scenarios for the microscopical nature of transition $(a \Rightarrow b)$ at $h/3$ as proposed in the preceding section.

Since the islands may elastically relax during their evolution increasing lattice parameter towards the apex will be favored in general. However, a linear increase of germanium concentration could be excluded by comparison with respective simulations indicating a discrete concentration profile. In order to prove whether the growth transition $(a \Rightarrow b)$ (the change from {115} towards {111}-type facets, respectively) performs similar to the preceding *nonfaceted* or to the subsequent *faceted* growth mechanism the particular germanium content has been used as a sensitive probe. Both models assume a fixed germanium content of 30% within $h \geqslant h/3$.

The simulation shown in Fig. 5(c) considers a truncated pyramid of 25% Ge covered by $Si_{0.7}Ge_{0.3}$—a linear and only height-dependent germanium gradient, which has been already proposed for LPE-SiGe islands.[10] However, in the present paper we compare this with a more sophisticated germanium distribution shown in Fig. 5(a) an embedded pyramid of 25% within the island bottom surrounded by a $Si_{0.7}Ge_{0.3}$ matrix. The recently reported three-dimensional concentration profile inside MBE-grown SiGe islands on Si(001) obtained by selective etching technique proves a higher germanium content around the island apex (compared with that in the island corners) as well.[19] *A priori* this particular distribution does not exclude the two models proposed here because crystal growth from the liquid phase provides different growth conditions rather close to thermodynamic equilibrium. This leads to—as the most obvious feature— different planar island orientations and corresponding faceting for MBE- and LPE-SiGe islands, which could motivate various concentration profiles as well.

Due to the models' particular inner structure the respective averaged germanium contents $\bar{x}$ hold $\bar{x}^a > \bar{x}^c$. Consequently, the center of diffuse intensity shifts from around $q_{001}^a = 4.555$ Å^{-1} towards $q_{001}^c = 4.560$ Å^{-1}.

In order to avoid any subjectivism when comparing experiment and respective simulations, a quantitative correlation analysis has been used. First of all it is noteworthy to state that simulations due to the finite size of our finite ele-

ment models, will be unable to reproduce a narrow crystal truncation rod. Also the ratio between the integrated intensities of x-ray scattering from the islands and substrate is not accessible by our calculations. Moreover, the most distinctive features of the diffuse scattering from islands are located apart from the substrate Bragg peak. Therefore, we have defined a range of interest for the correlation analysis. Taking into account the symmetry of reciprocal space intensity distribution for the 004 reflection with respect to the q_{001} axis, we have limited ourselves to a rectangular region defined by $q_{001} = 4.52 \cdots 4.56$ Å^{-1} and $q_{100} = 0.006 \cdots 0.030$ Å^{-1}.

The correlation coefficients have been calculated according to the conventional definition,

$$K(\xi, \eta) = \frac{cov(\xi, \eta)}{\sqrt{V\xi}\sqrt{V\eta}} = \frac{E((\eta - E\eta)(\xi - E\xi))}{\sqrt{E(\eta - E\eta)^2}\sqrt{E(\xi - E\xi)^2}}, \quad (3)$$

where ξ and η are the experimental and simulation datasets, respectively, $cov(\eta, \xi)$ denotes the covariance, and finally V and E are the variance and mathematical expectation value, respectively. Basically, the modulus of the correlation coefficient K is equal to one in the case of a linear dependence between datasets and is equal to zero in the case of purely independent datasets. Additionally, the correlation coefficient, due to the generic properties of mathematical expectations, is a noise proof. So, the correlation analysis could be performed on the raw data without any scaling adjustment. In order to reveal the minor features of the reciprocal space intensity distribution, intensities should be, naturally, represented in a logarithmic scale. However, the dynamical range of the experimental data is rather limited. The weak diffusely scattered intensities are superimposed by a background intensity, while the simulations are free of this experimental feature. This fact enforces us to shift the calculated intensity maximum to the experimental one in the region of interest, and to add a smooth experimental background. The given procedure was absolutely identical for both island models, including scaling coefficient and background level. Corresponding correlation coefficients were calculated, line by line along the q_{001} direction in the mentioned range of interest. Standard subroutines of two-dimensional interpolation, with averaging over q_{001} range, and vice versa were used.

Finally, we obtained K values of 0.84 for the model in Fig. 5(c) and a distinctly smaller value of 0.60 for the model in Fig. 5(a).

This difference is mainly caused by regions at q_{001} smaller than 4.54 Å^{-1}, which are comparatively far away from diffuse maxima, and are sensitive for the particular three-dimensional germanium distribution. For these regions alone the corresponding K values are 0.78 [Fig. 5(c)] and 0.32 [Fig. 5(a)]. This result indicates a growth mode for the transition $(a \Rightarrow b)$, which is rather similar to the growth via different side facets up to $\{115\}$.

In order to estimate the absolute accuracy of our treatment two-dimensional reciprocal space maps (RSM) based on objects similar to model Fig. 5(c) have been calculated, however, taking into account slightly different germanium contents. The final intensity distribution arising from a coherent summation of various RSM's shows a significant change with respect to the measured distribution only in case the absolute germanium content changes more than $\pm 1\%$. Thus, there is no indication to a concentration spread along different islands within the island ensemble.

VI. CONCLUSION

LPE grown self-organized $Si_{1-x}Ge_x/Si(001)$ islands have been investigated by means of direct imaging techniques as well as diffuse x-ray scattering.

Scanning electron micrographs address the well-known phenomenon of a finite island size during SK-growth mode to a twofold nucleation problem at the island bottom: (i) areas of exceptional high strain energy in vicinity of the island corners predicted by FEM calculations acts as a lateral nucleation barrier for the outmost $\{111\}$-type slabs, and finally, (ii) a strain driven wetting layer depression completely prevents ongoing nucleation at the island bottom.

Various growth stages observed by *ex situ* AFM at germanium contents below 15% reveal a three-step island nucleation process, wherein the island shape undergoes a significant change at one third of the final height from a lenslike type towards facetted islands. Since the incorporated germanium content probes the particular growth mode we applied HRXRD along with kinematical scattering simulations at samples where temporary growth stages could not be observed. From a discrete concentration change at exactly $h/3$ we conclude that the proposed island nucleation process remains the same even in case of higher concentrations.

[1] D. Bimberg, M. Grundmann, F. Heinrichsdorff, N.N. Ledentsov, Ch. Ribbat, R. Sellin, Zh. Alferov, P.S. Kopev, M.V. Maximov, V.M. Ustinov, A.E. Zhukov, and J.A. Lott, in *Nanoscale Linear and Nonlinear Optics*, edited by M. Bertolotti, C. M. Bowden, and C. Sibilia, AIP Conf. Proc. No. **560** (AIP, Melville, NY, 2001), p. 178.

[2] H. Ishikuro and T. Hiramoto, Appl. Phys. Lett. **71**, 3691 (1997).

[3] H. Okada and H. Hasegawa, Jpn. J. Appl. Phys., Part 1 **40**, 2797 (2001).

[4] I. Stranski and L. Krastanow, Sitzungsber. Akad. Wiss. Wien, Math.-Naturwiss. Kl., Abt. 2B **146**, 797 (1937).

[5] S.A. Chaparro, Y. Zhang, and J. Drucker, Appl. Phys. Lett. **76**, 3534 (2000).

[6] C.J. Huang, Y.H. Zuo, D.Z. Li, B.W. Cheng, L.P. Luo, J.Z. Yu, and Q.M. Wang, Appl. Phys. Lett. **78**, 3881 (2001).

[7] S. Christiansen, M. Albrecht, H.P. Strunk, and H.J. Maier, Appl. Phys. Lett. **64**, 3617 (1994).

[8] M. Cazayous, J. Groenen, F. Demangeot, R. Sirvin, M. Caumont, T. Remmele, M. Albrecht, S. Christiansen, M. Becker, H.P. Strunk, and H. Wawra, J. Appl. Phys. **91**, 6772 (2002).

[9] A.A. Darhuber, P. Schittenhelm, V. Holý, J. Stangl, G. Bauer, and G. Abstreiter, Phys. Rev. B **55**, 15 652 (1997).

[10] T. Wiebach, M. Schmidbauer, M. Hanke, H. Raidt, R. Köhler, and H. Wawra, Phys. Rev. B **61**, 5571 (2000).

[11] I. Kegel, T.H. Metzger, A. Lorke, J. Peisl, J. Stangl, G. Bauer, J.M. Garcia, and P.M. Petroff, Phys. Rev. Lett. **85**, 1694 (2000).

[12] K. Zhang, C. Heyn, W. Hansen, T. Schmidt, and J. Falta, Appl. Phys. Lett. **76**, 2229 (2000).

[13] M. Rauscher, R. Paniago, H. Metzger, Z. Kovats, J. Domke, J. Peisl, H.D. Pfannes, J. Schulze, and I. Eisele, J. Appl. Phys. **86**, 6763 (1999).

[14] Z. Kovats, M. Rauscher, H. Metzger, J. Peisl, R. Paniago, H.D. Pfannes, J. Schulze, I. Eisele, F. Boscherini, and S. Ferrer, Phys. Rev. B **62**, 8223 (2000).

[15] J. Stangl, A. Daniel, V. Holý, T. Roch, G. Bauer, I. Kegel, T.H. Metzger, T. Wiebach, T. Schmidt, and O.G. Eberl, Appl. Phys. Lett. **79**, 1474 (2001).

[16] R. Paniago, H. Metzger, M. Rauscher, Z. Kovats, J. Peisl, J. Schulze, I. Eisele, and S. Ferrer, J. Appl. Crystallogr. **33**, 433 (2000).

[17] A.J. Steinfort, P.M.L.O. Scholte, A. Etterna, F. Tuinstra, M. Nielsen, E. Landemark, D.-M. Smilgies, R. Feidenhans'l, G. Falkenberg, L. Seehofer, and R.L. Johnson, Phys. Rev. Lett. **77**, 2009 (1996).

[18] M. Schmidbauer, M. Hanke, and R. Köhler, Cryst. Res. Technol. **37**, 3 (2002).

[19] U. Denker, M. Stoffel, and O.G. Schmidt, Phys. Rev. Lett. **90**, 196102 (2003).

[20] N. Liu, J. Tersoff, O. Baklenov, A.L. Holmes, and C.K. Shih, Phys. Rev. Lett. **84**, 334 (2000).

[21] W. Dorsch, H.P. Strunk, H. Wawra, G. Wagner, J. Groenen, and R. Carles, Appl. Phys. Lett. **72**, 179 (1998).

[22] D.A. Faux, J.R. Downes, and E.P. O'Reilly, J. Appl. Phys. **82**, 3754 (1997).

[23] Q. Shen and S. Kycia, Phys. Rev. B **55**, 15 791 (1997).

[24] V.M. Kaganer and K.H. Ploog, Phys. Rev. B **64**, 205301 (2001).

[25] G.S. Pearson and D.A. Faux, J. Appl. Phys. **88**, 730 (2000).

[26] T. Benabbas, P. Francios, Y. Androussi, and A. Lefebvre, J. Appl. Phys. **80**, 2763 (1996).

[27] M. Grundmann, O. Stier, and D. Bimberg, Phys. Rev. B **52**, 11 969 (1995).

[28] Program package MarcMentat©.

[29] L. Vegard, Z. Phys. **5**, 17 (1921).

[30] S. Christiansen, M. Albrecht, H.P. Strunk, P.O. Hansson, and E. Bauser, Appl. Phys. Lett. **66**, 574 (1995).

[31] M. Hanke, Ph.D. thesis, Humboldt-Universität zu Berlin, Mensch & Buch Verlag, ISBN 3-89820-398-0, 2002.

[32] W. Dorsch, B. Steiner, M. Albrecht, H.P. Strunk, H. Wawra, and G. Wagner, J. Cryst. Growth **183**, 305 (1998).

[33] X.Z. Liao, J. Zou, X.F. Duan, D.J.H. Cockayne, R. Leon, and C. Lobo, Phys. Rev. B **58**, R4235 (1998).

[34] U. Denker, O.G. Schmidt, N.Y. Jin-Phillip, and K. Eberl, Appl. Phys. Lett. **78**, 3723 (2001).

[35] X.Z. Liao, J. Zou, D.J.H. Cockayne, J. Qin, Z.M. Jiang, X. Wang, and R. Leon, Phys. Rev. B **60**, 15 605 (1999).

[36] X.Z. Liao, J. Zou, D.J.H. Cockayne, Z.M. Jiang, X. Wang, and R. Leon, Appl. Phys. Lett. **77**, 1304 (2000).

[37] M. Hanke, H. Raidt, R. Köhler, and H. Wawra, Appl. Phys. Lett. **83**, 4927 (2003).